Lab on a Chip

PAPER

View Article Online
View Journal

Cite this: DOI: 10.1039/c9lc00163h

Traveling surface acoustic wave (TSAW) microfluidic fluorescence activated cell sorter (μFACS)†

K. Mutafopulos, [a] P. Spink, [a] C. D. Lofstrom,[b] P. J. Lu, [ac] H. Lu,[a] J. C. Sharpe,[b] T. Franke [d] and D. A. Weitz *[ac]

Received 15th February 2019,
Accepted 4th June 2019

DOI: 10.1039/c9lc00163h

rsc.li/loc

We report a microfluidic fluorescence activated cell-sorting (μFACS) device that employs traveling surface acoustic waves (TSAW) to sort cells at rates comparable to conventional jet-in-air FACS machines, with high purity and viability. The device combines inertial flow focusing and sheath flow to align and evenly space cells, improving the sorting accuracy and screening rate. We sort with an interdigital transducer (IDT) whose tapered geometry allows precise positioning of the TSAW for optimal cell sorting. We sort three different cell lines at several kHz, at cell velocities exceeding one meter per second, while maintaining both sorting purity and cell viability at around 90% simultaneously.

Introduction

Conventional fluorescence activated cell-sorting (FACS) is a valuable and widely-used tool in molecular and cellular biology, which optically screens each cell and encapsulates it into an aerosolized droplet that is charged so that it can be electrostatically deflected to be sorted. However, despite its utility and wide-spread applicability, FACS has some unavoidable drawbacks that can be eliminated by sorting with a microfluidic device. As a bulk technique with millimeter sized components, FACS requires orders of magnitude larger sample volumes[1] than microfluidic devices with micron sized channels, to achieve similar yields.[2–7] Microfluidic fluorescent activated cell sorters (μFACS) eliminate the use of an aerosol nozzle that can damage cells or create safety concerns when handling infectious cells.[8] Furthermore, microfluidic devices are much easier to align optically and are disposable, eliminating potentially biohazardous clean-up steps that a FACS machine requires after each use.[2,3,6,9] Lastly, the channel geometries of microfluidic devices can be curved to utilize the inertial effects of fluid flow to control cell position, which facilitates high-throughput analysis.[10,11] Several cell-sorting mechanisms have been used in microfluidic devices, including piezoelectric actuation, surface acoustic waves (SAW), and pulsed laser-activated cell sorting (PLACS). Each of these techniques sort at rates that are comparable to FACS, offering an attractive alternative;[2–5,7,12–16] for example, PLACS can achieve 90% purity at 1000–3000 events per second,[5,13] but creates cavitation bubbles in the channel that potentially harm cells. Moreover, standing surface acoustic waves (SSAW) have demonstrated the ability to focus and sort 2500 cells per second while achieving 90% purity.[7] However, the SSAW wavelength is fundamentally determined by the device geometry, constraining the range of its application and precluding adjustment after device fabrication.

By contrast, traveling surface acoustic waves (TSAW) deflect cells into a separate channel with no wavelength constraint *via* acoustic radiation[3] and streaming,[4] thus facilitating TSAW integration with a wide variety of channel geometries without modification.[3,4,14,17] Despite this advantage, TSAW has not thus far demonstrated microfluidic cell sorting under high-speed conditions with switch cycles fast enough to achieve sorting rates comparable to FACS; the ability to sort cells rapidly using a microfluidic device has the potential to replace conventional FACS machines, providing users with smaller scale devices that are disposable and can handle small volumes.

In this paper, we report a μFACS device that combines a spiral channel for inertial flow focusing with a tapered interdigital transducer (IDT) that generates a 25 μs TSAW pulse to rapidly deflect cells into a separate channel upon fluorescence detection. We sort cells at rates up to 5000 events per second while maintaining cell viability in excess of 90%; moreover, at rates up to 2000 events per second, we maintain sorting purity above 90%, comparable to FACS. Our device, which for our TSAW pulse duration has a theoretical

[a] School of Engineering and Applied Sciences, Harvard University, Cambridge, MA, 02138, USA. E-mail: weitz@seas.harvard.edu
[b] Cytonome/ST, LLC, Bedford, MA, 01730, USA
[c] Department of Physics, Harvard University, Cambridge, MA, 02138, USA
[d] Biomedical Engineering, School of Engineering, University of Glasgow, GlasgowG12 8QQ, UK

† Electronic supplementary information (ESI) available. See DOI: 10.1039/c9lc00163h

maximum sorting rate of 40 kHz, demonstrates the high sorting performance capabilities of TSAW-based FACS and provides an attractive alternative to conventional sorting methods.

Results and discussion

Our cell-sorting device is composed of polydimethylsiloxane (PDMS) molded microchannels bonded to a lithium niobate substrate containing a tapered IDT. We pattern the IDT onto 128° Y–X lithium niobate, which serves as the piezo-electric material to create TSAWs, as well as the substrate to seal the PDMS device. To optimize TSAW sorting, the cells are spatially ordered in a straight line and positioned close to the surface of the lithium niobate substrate side of the channel to guarantee interaction with the pulsed acoustic wave in the sorting region. To accomplish this, cells entering the device first flow through a spiral channel, which inertially flow focuses them into a single ordered line, as shown in Fig. 1a and Video S1.† We use a spiral channel, since fluid flowing through this channel geometry experiences centrifugal acceleration, creating two counter-rotating Dean vortices in the top and bottom halves of the channel.[10,11,18–23] These vortices position cells in the fluid into a nearly evenly-spaced single file.[11,18–21,24,25] To ensure the spiral channel can inertially focus cells that are 10 to 15 μm in diameter, we set the hydraulic diameter of the channel, defined as $D_h = 2hw/(h + w)$ where h and w are the height and width of the channel cross section, respectively, to 51 μm, to satisfy the particle confinement ratio inequality, $\lambda > 0.07$, where λ is the ratio between particle diameter and hydraulic radius.[10,21] These parameters efficiently focus particles larger than 4 μm. Furthermore, we set the flow rate in the channel to 1.5 mL per hour, corresponding to a Reynolds number of approximately 17, and the length of the spiral channel to 61.5 mm, in accordance to design rules for inertial focusing within our device dimensions.[11] Although spiral channels have been used to sort objects by size,[18] our cells are sufficiently monodisperse so that we observe no size segregation at the spiral exit.

At the exit of the spiral, our cells are confined into a narrow region laterally in the center of the flow, as shown in panel 3 of Fig. 1a; to confine further their vertical placement, we add a vertical flow-focusing nozzle, a multi-layer feature which introduces a vertical constriction at the intersection with the two sheath-flow channels, as shown in Fig. 1b. The vertical constriction focuses the cells into a narrow sample core stream towards the bottom of the channel, maximizing the interaction of cells with the acoustic wave.[3,26] Additionally, the sheath flow further separates the cells and positions them within the sorting region, as shown in Fig. 1b. Upon entering the sorting region, the cells are illuminated by a 473 nm laser to excite fluorescence in labeled cells; the fluorescent light is detected by a photomultiplier tube (PMT) and triggers a signal generator to activate the IDT. The IDT induces a 25 μs TSAW pulse that deflects the fluorescent cells into a separate keep channel, as shown schematically in Fig. 1c. When the IDT is not activated, cells flow unaffected through the sorting region and into the waste outlet channel. A microscope image of the sorting region, with the IDT and outlet channels is shown in Fig. 2 and Video S2.† The combination of inertial and vertical flow focusing features together guide cells to enter the sorting region one at a time for localized and precise cell-acoustic wave interaction for reproducible cell deflection.

A radio frequency (RF) signal of 162 to 164 MHz is applied to the IDT, generating a TSAW that is refracted into the sorting region of the fluid channel adjacent to the IDT, leading to a deflection of the detected cell into the keep channel, as shown in Fig. 1c. At these frequencies, 10–15 μm cells are deflected by acoustic radiation forces, not streaming.[27] We taper the electrode pairs of the IDT to allow the adjustment of the TSAW position along the direction of flow in the channel (x-direction in Fig. 1c) by tuning the RF of the signal generator,[28–31] ensuring optimal cell deflection and

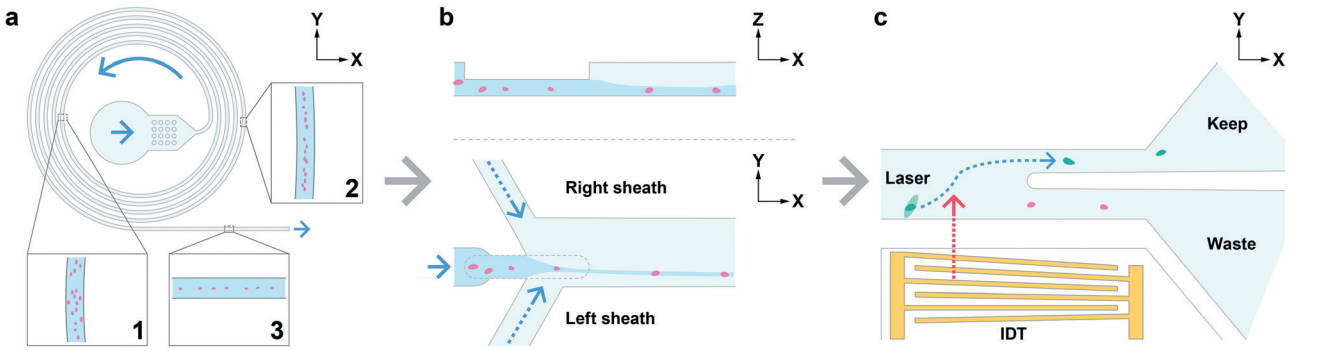

Fig. 1 Overview of the sorting device. (a) Cells are flowed through a spiral microchannel to focus and align the cells into a single file. The spiral channel causes cells to experience both inertial migration and influences from Dean vortices, minimizing the number of positions a cell can occupy in the channel. By minimizing the number of positions, the likelihood that cells will deviate from the desired flow path, an event known as misfocusing, is minimized.[13] (b) The outlet of the spiral channel connects to a vertical flow focusing nozzle flanked by two sheath flow channels at higher flow rates than the spiral channel to accelerate, further align, and space cells upon entering the sorting region and to further minimize misfocusing events. (c) Cells are sequentially interrogated by a laser and detector in the sorting region. Cells that are fluorescently labeled are detected and deflected into a separate channel (keep) by the IDT.

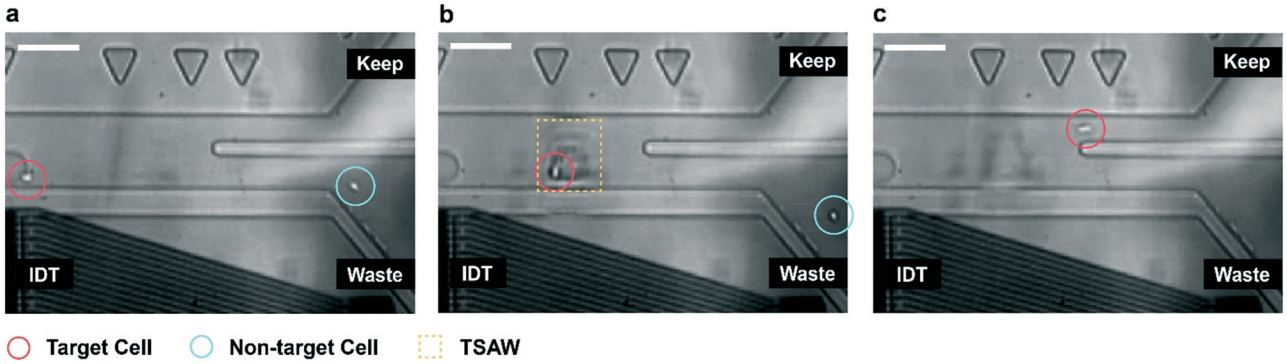

Fig. 2 Individual frames from a high-speed camera video recording (10 000 fps) of a fluorescently labeled Mycl-9E10 cell being sorted by the traveling acoustic wave (flow direction is from left to right). (a) Fluorescently labeled cell, circled in red, enters the sorting region and is detected. A non-fluorescently labeled cell, circled in blue, is shown entering the waste outlet channel as the fluorescently labeled cell enters the sorting region. (b) When a cell is detected, 12.5 W of power is applied to the IDT to generate a traveling surface acoustic wave for 25 μs into the sorting region. (c) Deflected cell entering the keep outlet channel after interacting with the applied TSAW. Scale bar is 100 μm.

compensation for slight variations in IDT alignment from fabrication. The IDT is placed beneath an air pocket separate from the fluid in the sorting region, to prevent acoustic waves from leaking into the PDMS device. The thickness of the PDMS separating the air gap from the liquid in the sorting region is minimized to reduce power loss. When the TSAW impinges on the interface of a fluid it refracts and establishes longitudinal acoustic waves in the fluid;[3,32–34] these waves deflect cells by acoustic radiation forces into a separate outlet channel.[15,27,35]

For all experiments the flow rates are held constant to maintain a uniform flow velocity. The sample flow rate is 1.5 ml per hour, while the left and right sheath flow rates are 4 and 8.5 ml per hour respectively. The right sheath fluid operates at a higher flow rate to direct cells entering the sorting region into the waste outlet channel when the IDT is off. We compare three

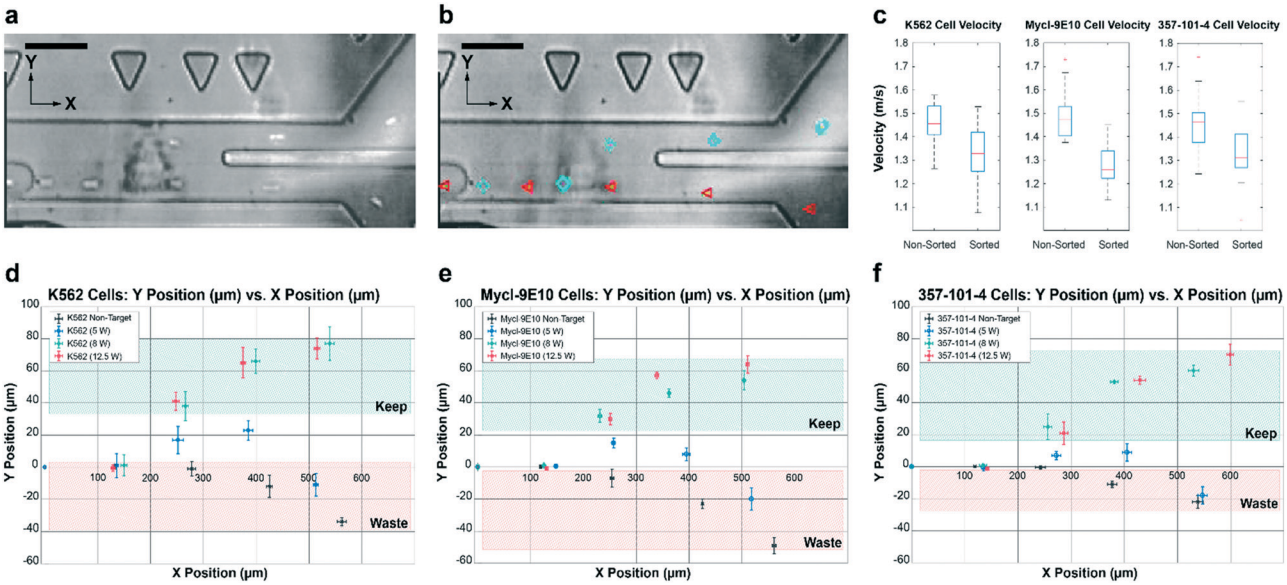

Fig. 3 High-speed camera videos are captured as unlabeled (non-target) and fluorescent labeled cells (target) flow through the sorting region. Triangles adjacent to sorting channel region are used for laser positioning, TSAW positioning, and particle tracking reference points. Videos are analyzed in Tracker to map the 2-D position of cells sorted at 5 W, 8 W, and 12.5 W. Scale bars are 100 μm (a) multiple frames from a sort event are superimposed to create an image depicting the trajectory of a sorted and non-sorted cell (cells in image are Mycl-9E10) (b) multiple frames from (a) after Tracker analysis super imposed to create in image depicting Tracker analysis. (c) Average velocity measurements for all three cell lines in the sorting region. Individual cell velocity measurements are obtained from high-speed camera videos analyzed and averaged using Tracker. Both target and non-target cells are measured for comparison. Sorted cells experienced a lower velocity on average due to deflection into the keep outlet channel. (d–f) Normalized cell deflection plots for all three cell lines under the same flow conditions (flow direction is from left to right). (d) K562 normalized *X* and *Y* position in the sorting junction for non-target and target cells deflected at 5 W, 8 W, and 12.5 W. (e) Mycl-9E10 normalized *X* and *Y* position in the sorting junction for non-target and target cells deflected at 5 W, 8 W, and 12.5 W. (f) 357-101-4 normalized *X* and *Y* position in the sorting junction for non-target and target cells deflected at 5 W, 8 W, and 12.5 W. Error bars represent confidence intervals.

different IDT power levels to determine the amount of power needed to deflect cells successfully at high speeds. We repeat each power-setting experiment five times across four separate chips to quantify reproducibility, and test against three different cell lines: K562 (ECACC 89121407), Mycl-9E10 (ECACC 85102202), and 357-101-4 (ECACC 92030603) cells. We record high-speed videos of cells flowing through the sorting region; we track individual cell positions using open-source tracking software (Tracker, Open Source Physics, physlets.org/tracker), quantifying cell velocity and deflection. In each of the experiments, we reconstruct the trajectories of an average of twenty cells through the sorting region.

Cell velocity and deflection

To demonstrate the high-speed capabilities of our sorting device, we record high-speed videos of cells entering and exiting the sorting region at 10 000 FPS and use the tracking software to measure the average velocity of sorted and non-sorted cells in the direction of flow (x-component) in the sorting region as shown in Fig. 3a and b. We find the average x-component velocity for non-sorted cells of all three cell lines is close to 1.5 m s^{-1}. We do not observe a large variation in velocity for non-sorted cells since the cells are run under the same flow conditions and are of similar size; using a commercial cell counter (Countess FL II Automated Cell Counter, ThermoFisher, Waltham, MA) we find that the average cell diameters of the K562, Mycl-9E10, and 357-101-4 cells are approximately 15 μm,[36] 10 μm, and 10 μm, respectively. For sorted cells of these types, we find the average x-component velocity to be approximately 1.3 m s^{-1}; this slight decrease in velocity is a result of the sorted cells being deflected vertically and laterally across the sorting region away from their mean flow path.[3] The average x-component velocity measurements are shown in Fig. 3c.

We actuate the IDT at three different power levels to determine the amount of power required to successfully deflect a target cell away from the mean flow path and into the keep channel. We observe that increasing the power applied to the IDT increases the amount of deflection a cell experiences in the sorting region. A supply of 5 W of power or less to the IDT does not deflect a cell into the keep channel, while a supply of 8 W or 12.5 W to the IDT does successfully deflect cells. For each of the IDT power settings, we normalize, and plot for each cell line the 2-D position of sorted and non-sorted cells in the sorting region as shown in Fig. 3d–f. We observe that at 12.5 W, the Mycl-9E10 cells are deflected slightly further in the Y-direction than at 8 W; therefore, we actuate the IDT at 12.5 W for all velocity measurements, purity performance experiments, and cell viability measurements. These observations in cell deflection correlate with the widely discussed coherence between particle deflection and the IDT input power.[14,37–39]

Sorting purity

For purity measurements, we label 10% of the total number of cells with calcein AM fluorescent dye and sort them from non-labeled cells for all event rates. We count cells obtained from the keep channel using the commercial cell counter to determine the percentage of stained cells present. We repeat purity experiments ten times at each event rate condition for all three cell lines, and use a different microfluidic chip for each experiment to determine reproducibility.

We adjust the cell event rate by changing the concentration of cells processed through the sorting device while maintaining the same flow conditions. We define the event rate here as the projected number of cells entering the sorting region per second, which we estimate based on the total number of cells and sample flow rate. At low event rates the sorting device accomplishes high purity, but the purity declines as the event rate is increased; we observe that all three cell lines follow a similar decrease in purity as the event rate increases, as shown in Fig. 4. We observe that as the cell concentration rises, the probability of more than one cell being present during a sorting event also increases; in these coincident events, multiple cells are deflected into the keep channel at the same time, decreasing the purity. At the flow rates and cell concentrations we use, coincident events become noticeable when more than one cell arrives in the sorting region within 100 μs. In commercial FACS machines, higher levels of purity are obtained by the detection and elimination of such coincident events; introducing coincident event detection software, as commonly found in conventional

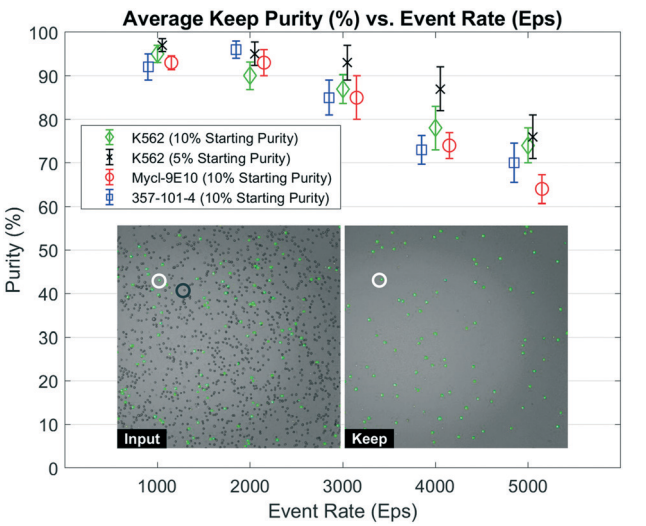

Fig. 4 Purity performance of the sorting device for each cell line. Data for 10% starting purity shown with open symbols: K562 (green diamonds), Mycl-9E10 (red circles), 357-101-4 (blue squares). The average keep purity of each recovered sample is plotted relative to the cell line and event rate. Each data point represents the average from 10 sorting runs and the error bars represent confidence intervals. Cells obtained from the keep outlet are measured on the Countess FL II to determine the fraction of fluorescent cells present. Event rate is controlled by adjusting cell concentration of the sample. Sorting purity increases with decreased starting purity, shown for K562 cells at 5% starting purity (black crosses) (insert) Countess FL II images of 357-101-4 cells before and after sorting at 2000 events per second. White circle indicates fluorescent labeled cells, black circle indicates non-labeled cells.

Table 1 Average cell viability measurements for each cell line. Viability was determined by trypan blue and measurements were made on the countess FL II. Input is defined as cell viability prior to sorting. The keep and waste are viability measurements of sorted and non-sorted cells respectively. Control is defined as a fraction of cells from the input placed on ice and never introduced into the device but measured after the sorting run

Cell line	K562	Mycl-9E10	357-101-4
Average viability live%			
Input	95.8 ± 2.0	96.8 ± 1.0	96.5 ± 1.8
Keep	91.4 ± 2.9	91.8 ± 2.9	91.6 ± 3.8
Waste	93.1 ± 2.4	93.4 ± 3.4	93.6 ± 2.9
Control	95.0 ± 1.7	94.4 ± 2.8	95.4 ± 2.3

FACS instruments, would likely maintain sorting purity above 90% at all tested event rates.

Viability

To assess cell viability, we stain cells with 0.4% trypan blue (Thermo Fisher Scientific, USA) and quantify the percentage of live and dead cells using the commercial cell counter, sorting with the same power and pulse settings. We collect four cell viability measurements during eight sorting runs for each cell line to determine if cell viability is affected by the acoustic wave, the sorting device, or both. We measure cell viability prior to loading the cell suspension into the sorting apparatus. During a sorting run, we extract fractions of the keep and waste for viability measurements.

We then obtain a fourth viability measurement from a fraction of the same cell solution used for the sorting experiment that is never loaded into the sorting apparatus as a control. We observe a small decrease in viability of a few percent for the keep cells in comparison to the input, waste, and control viability measurements, as summarized in Table 1. We attribute this small decrease due the fact that cells collected from the keep collection tubes are centrifuged and resuspended to provide a higher concentration of cells for accurate measurements using the commercial cell counter. It is also possible that this small decrease is due to the amount of power used to deflect fluorescent labeled cells. Further studies would be required to determine if increased acoustic power would decrease cell viability.

Conclusions

We demonstrate a microfluidic cell sorter that integrates inertial and hydrodynamic flow focusing with a TSAW to sort cells at throughputs comparable to conventional FACS. The device sorts cells and obtains sort purities in excess of 90% for event rates up to 2000 events per second using a 25 μs acoustic wave pulse. We measure cell viability for three different live cell lines to demonstrate the gentleness of acoustic sorting. Our sorting device keeps all liquids enclosed and generates no aerosols, enabling applications that involve biohazardous samples. The sorting device could be improved by implementing coincident event logic software to discard cells that are too close together to be sorted individually, potentially maintaining purity above 90% at sorting rates exceeding 3000 events per second. Microfluidic devices that use TSAW for cell sorting may have a broad spectrum of research and industrial applications such as cancer research,[40] reproductive technologies,[41] and rare cell enrichment.[42]

Materials and methods

Soft lithography

The polydimethylsiloxane (PDMS) molded microfluidic channels of the device are comprised of two layers, each fabricated using a separate photomask. The first layer comprises of the vertical flow-focusing nozzle. The nozzle is designed to be nominally 190 μm long and extends underneath both the sample inlet and the sorting region. The second layer contains the sample and sheath inlet channels, the sorting region, the device outlets, and the IDT air pocket. The sample inlet consists of a 70 μm wide by 61.5 mm long spiral channel with five consecutive turns that leads to the sorting region. The sheath channels form a *Y*-shape with the sorting region to prevent stagnation points as flow emerges from the nozzle. The nozzle and sample inlet are offset from the center of the sorting region to ensure cells will not enter the keep outlet channel unless deflected by the pulsed acoustic wave. The air pocket is a rectangular shaped area that prevents acoustic waves from leaking into the PDMS device away from the intended sort region. The thickness of the PDMS separating the air pocket from the liquid in the sorting region is minimized while maintaining fluidic sealing to 50 μm to reduce power loss. Each layer contains two sets of alignment marks consisting of an asymmetrical pattern of crosses,[43] enabling the two layers to be aligned precisely. The masks for the individual layers were ordered from CAD/Art Services, Inc. (Bandon, OR) and imaged with a resolution of 15 400 dpi.

We perform multi-layer lithography to create molds for PDMS replicas. We process the layers by following the method recommended in the manufacturer's data sheet for SU-83000 series photoresists (MicroChem Corp., Westborough, MA). For each layer, we dispense a small amount of SU-83025 photoresist (MicroChem) onto the silicon wafer. We spin the wafer at 4000 rpm to create a layer that is 20 μm thick. We pre-bake each layer for a total of 12 minutes at 95 °C on the hot plate. We use a contact mask aligner (ABM, Scotts Valley, CA) to align and pattern with UV light any underlying features to the photomask (CAD/Art Services Inc., Bandon, OR). We then post-exposure bake the resist for 1 minute at 65 °C and 5 minutes at 95 °C, followed by immersing the wafer in polyethylene glycol monomethyl ether acetate (484431, Sigma-Aldrich Co. LLC, St. Louis, MO) for 6 minutes using an orbital shaker (Roto Mix 8 × 8, Thermo Fisher, Waltham, MA) for mixing. After development, we rinse the wafer with isopropanol and blow dry it with compressed nitrogen. We repeat these steps for each subsequent layer. After the layers have been developed, the wafer is

now ready to serve as a mold for creating PDMS replicas. The layers result in a channel depth of 40 μm for all channels except the vertical flow-focusing nozzle, which is 20 μm in depth.

We mix PDMS (Sylgard 184, Dow-Corning, Midland, MI) base and cross-linker in a 10 : 1 weight ratio using a Thinky mixer (AR-100, Thinky Corp., Tokyo, Japan). We de-gas the PDMS for 20 minutes and cure the mold in the oven at 65 °C overnight to create a replica. We cut the PDMS replica into individual devices prior to use. We create inlet- and outlets holes with a 1.2 mm diameter biopsy punch (Uni-Core, GE Healthcare Life Sciences, Pittsburgh, PA). Next, we bond individual devices to the lithium niobate substrate using an oxygen plasma stripper (PE-50, Plasma Etch, Carson City, NV). During the bonding procedure, we align the PDMS device to the IDT so that the electrodes are situated beneath the air pocket, to prevent the acoustic waves from leaking into the PDMS device prematurely. The PDMS device forms three sides of the device's flow channel, while the lithium niobate substrate serves as the bottom of the flow channel.

Interdigital transducer (IDT)

The device uses an IDT with a tapered-finger design.[31] The design is characterized by a continuously changing pitch of the IDT fingers from one side to the other; effectively varying the position of the resonant frequency laterally along the transducer. Our IDT resonant frequency ranges from 160 to 172 MHz.[44] The excited SAW beam of the resonance region can be approximated by the electrode aperture and the frequency difference between each IDT pole.[31] The average wavelength is approximately 25 μm and the beam width is approximately 30 μm in our design. The metallization ratio, a/p, which is the fraction of the electrode width, a, and pitch, p, is 0.5 throughout the transducer. Electrodes on either pole are interconnected by trapezoidal bus bars that merge into square contact pads to apply external voltages. The trapezoidal bus shape prevents the IDT from obstructing the flow channels of the PDMS slab.

We fabricate the IDTs in a lift-off process using a modified protocol from the Center for Nanoscale Systems at Harvard University. We use double polished 4″ diameter black 128° *Y–X* cut lithium niobate that is 500 μm thick as the piezoelectric substrate, because it offers adequate optical transparency, strong electro-mechanical coupling with low bulk wave generation and high SAW velocity.[31,45] In addition, the black, chemically reduced lithium niobate helps facilitating fabrication steps that involve baking on heat plates by effectively eliminating the pyroelectric effect.[46] We clean each wafer with acetone and isopropanol. We remove any residual moisture on the wafer with a dehydration bake on a heat plate at 180 °C for minimum 3 minutes. For every step involving baking, we hold the wafer 5 to 10 mm above the heat plate surface for about 20 seconds before placing it down, to ease temperature changes of the substrate and reduce the risk of cracking. Consequently, we hold hot wafers in air for about 20–30 seconds to gently cool down the substrate to room temperature before proceeding with any next steps. We create a 300 nm thick sacrificial layer by spin coating LOR 3A (MicroChem Corp., Westborough, MA) at 3000 rpm on the cleaned wafer surface, followed by baking the layer at 180 °C for 7 minutes. Subsequently, we spin Shipley S1805 (MicroChem Corp., Westborough, MA) at 4000 rpm to form a 500 nm layer of photoresist on top of the sacrificial layer and baked for 1 minute at 115 °C.

We expose the coated wafers to a UV dosage of 40 mJ cm^{-2} and a wavelength of 405 nm using a mask-less alignment tool (MLA150, Heidelberg Instruments, Germany) to transfer the designed IDT patterns to the substrate. We develop the exposed patterns in CD-26 developer (Microposit MF, Dow Electronic Materials, Marlborough, MA) during a 75-second-long immersion, followed by a rinse with deionized water and drying the wafer with nitrogen. Prior to metal deposition, we clean wafers with oxygen plasma for 3 minutes at 150 W and 40 sccm gas flow (Anatech SCE-106 plasma barrel etcher, Anatech USA, Union City, CA) to remove organic residues from the substrate surface that could impair metal adhesion. We use electron beam physical vapor deposition (Denton Explorer 14, Denton Vacuum LLC, Moorestown, NJ) to create a 10 nm thick titanium adhesion layer, followed by 50 nm of gold to form IDTs on the wafer. To obtain the IDTs, the deposited wafers are soaked in a Remover-PG bath (MicroChem Corp, Westborough, MA) at 80 °C for about 3 hours to lift-off the sacrificial layer and cleaned with isopropanol.

To facilitate plasma bonding between the PDMS molded channels and the piezoelectric substrate, we coat the lithium niobate wafers containing the IDTs with a 50 nm layer of SiO_2 using a sputtering system (AJA International Inc., Scituate, MA). Prior to the sputtering process, we coat the electrode contact pads with a layer of Shipley S1813 (MicroChem Corp., Westborough, MA) and bake it for 2 minutes at 115 °C to prevent SiO_2 deposition onto the region of IDT that requires electrical contact. The protective layer is subsequently cleaned with oxygen plasma during 5 minutes at 150 W and 40 sccm gas flow.

We prepare wafers for post processing by spinning Shipley S1813 at 3000 rpm followed by baking at 115 °C for 2 minutes to form a protective layer. The substrate is scored with 250 μm deep lines using an automated dicing saw (DAD321, DISCO Corp., Tokyo, Japan) and then broken into individual, 17.4 mm × 17.4 mm squares each containing a single IDT. The protection layer and the contact pad coating are removed by soaking individual IDTs in acetone for about 15 minutes; cleaning them with isopropanol.

Sorter apparatus

The sorting apparatus is similar to what has been described in previous works,[3,47,48] and uses a custom-built microscope using modular optomechanical components (Thorlabs Inc., Newton, NJ). We expand and steer (BE-05-10-A, Thorlabs Inc.) a 473 nm laser with 100 mW of output power (LRS-0473,

Laserglow Technologies, Toronto ON), into the microscope to excite fluorescently labeled cells. A cylindrical achromat (ACY254-200-A, Thorlabs Inc.) and a microscope objective (Nikon CFI Plan Apochromat Lambda, 10X/0.45NA, Micro Video Instruments, Inc., Avon, MA) focus the laser beam into a line in the microscope's focal plane. Any fluorescence emitted by the cell is collected by the objective and the excitation light gets reflected by the excitation dichroic (FF495-Di03-25x36, Semrock, Inc., Buffalo, NY) and up through the objective, and the emitted fluorescence passes through the excitation dichroic. The fluorescence reflects off the fluorescence dichroic (FF757-DiO1-25x36, Semrock, Inc.) towards the photocathode of a photomultiplier tube (PMT) (H10723-20, Hamamatsu Photonics K.K., Hamamatsu Japan). We place a colored glass longpass filter (FGL495, Thorlabs Inc.) and a dielectric bandpass filter (FF01-520/44-25, Semrock, Inc.) between the fluorescence dichroic and the PMT to reduce noise sources of light to provide accurate measurements of fluorescence. To illuminate the microscope's field, we use a 850 nm light emitting diode (LED) (48 T1419, LZ1-30R400, Newark Element14, Chicago IL). The infrared light passes through both dichroic filters and is reflected by a steering mirror (CM1-P01, Thorlabs Inc.). The infrared image is focused onto the sensor of a high-speed camera (HiSpec1, Fastec Imaging, San Diego, CA) by a tube lens (AC254-100-B-ML, Thorlabs Inc.) The high-speed camera enables the system to record high framerate videos of the sorting process. A manual stage (Leica) provides adjustment of the sample position with respect to the optical system.

The PMT measures the fluorescence from the sample, generating a voltage proportional to the intensity of the measured light. The voltage is digitized by a data acquisition card (PCIe-7842R, National Instruments Corp., Austin TX) and analyzed in real time using the card's field programmable gate array to detect and analyze peaks in the fluorescence signal. When peaks corresponding to desired cells are detected, a 25 μs sorting pulse is generated. The sorting pulse a 3 V signal, which controls the output of a RF waveform generator (SMB100A, Rhode & Schwarz, Munich, Germany) through its pulse modulation input. The output is amplified using a high gain RF amplifier (LZY-22+, Mini-Circuits, Brooklyn, NY). When the amplified signal applied to the IDT, the IDT produces SAWs in response. We use a PC to set threshold values for peak detection and sorting, and to monitor system performance. Using this system, the fluorescence from cells passing through the sorting region of the device are analyzed in real time, and pulses of SAW are applied to sort desired cells with minimal latency. The microfluidic device is supported by a custom-made sample holder that fits into the microscope stage, and the base plate of the sample holder holds the lithium niobate containing the IDT of the chip securely. We cut away the center of the baseplate to permit light to transmit through the sample and to focus the microscope into the channels of the device. A glass slide is cut to size and placed under the IDT to provide mechanical support. A clear piece of lithium niobate is taped underneath the glass slide in an orientation chosen to cancel the effects of the birefringence. A printed circuit board (PCB) routes signals from the amplifier to the IDT. The amplifier and the PCB are connected using standard RF adaptors (SMA to MMCX male), and electrical connections from the PCB to the IDT are created when pogo pins mounted on the board are pressed into contact with the metal pads. The PCB is held in place by fixing it to the base plate using M3 screws. An acrylic spacer plate ensures that the pins exert enough contact force to hold the IDT in place and make consistent electrical contact. The spacer is milled to 3.7 mm and laser cut to accommodate the mounting screws, the shape of the PCB, and electrical components on the lower side of the PCB.

Deflection, purity, and viability characterization experiments

We harvest either K562 (ECACC 89121407), Mycl-9E10 (ECACC 85102202), or 357-101-4 (ECACC 92030603) cells prior to sorting experiments. We remove a fraction of the cell suspension and stain it by adding calcein AM (Life technologies, Grand Island, NY) to the cell suspension at a concentration of 1 μM and incubating the suspension at 37 °C for 20 minutes. Stained cells are re-suspended into injection buffer at or between 3 and 12 million cells per ml depending on event rate desired. Injection buffer consists of 1% Optiprep (D1556, Sigma-Aldrich Co. LLC) by volume, 6 U ml^{-1} DNAse I (New England Biolabs Inc., Ipwich, MA), 3 mM magnesium chloride, 10% fetal bovine serum (FBS) by volume in Dulbecco's Modified Eagle's Medium (DMEM, 10-013-CV, Corning). Mycl-9E10 and 357-101-4 cells are prepared the same with the exception that DMEM is replaced with Roswell Park Memorial Institute Medium (RPMI, R8758, Sigma-Aldrich). The flow rate of the cell phase is 1.5 ml h^{-1}, while the sheath fluid has a total flow rate of 12.5 ml h^{-1}. The sheath fluid is either DMEM with 10% FBS or RMPI with 10% FBS depending on the cell line used. The left sheath fluid comes from the inlet nearest the waste outlet at a flow rate of 4 ml h^{-1}, while the right sheath fluid comes from the inlet nearest the keep outlet at a flow rate of 8.5 ml h^{-1}. The right sheath fluid operates at a higher flow rate to flow cells into the waste channel when the IDT is inactive.

The frequency of the RF pulse used to produce TSAWs is tuned to the resonant frequency determined by the geometric and physical parameters of the IDT, substrate and device; we tune this frequency at or between 162 and 164 MHz depending on IDT alignment to the sorting junction during device fabrication. This ensures that the acoustic wave is produced at the approximately the same position in the sorting region for each deflection and purity experiment. Unless noted, no cells enter the keep channel unexpectedly for the conditions tested. High speed videos of individual sorting events are analyzed to determine whether a cell is successfully deflected into the keep outlet or not. We centrifuge and resuspend cells collected from the keep outlet channel to obtain higher a concentration for accurate purity counts using the Countess FL II.

We measure cell viability by mixing cells with 0.4% trypan blue stain (Thermo Fisher Scientific, USA) in a volume ratio of 9 to 1. Each sample incubates at room temperature for one minute prior to injection into a disposable cell count board. We then load the injected cell count board into the Countess FL II and record the percentage of unstained cells to the total cell number.

Conflicts of interest

There are no conflicts to declare.

Acknowledgements

This work was supported by the Harvard Materials Research Science and Engineering Center, National Science Foundation DMR-1420570, and Cytonome/ST, LLC (Bedford, Massachusetts). This work was performed in part at the Center for Nanoscale Systems (CNS), a member of the National Nanotechnology Coordinated Infrastructure Network (NNCI), which is supported by the National Science Foundation under NSF award no. 1541959. CNS is part of Harvard University. The authors would also like to thank John Heyman and Julie Brouchon for providing K562, Mycl-9E10, and 357-101-4 cells. KM and PS would especially like to thank Will Williams, and Eric Raborn for their advice, assistance, and helpful discussions.

Notes and references

1 H. M. Shapiro, *Practical Flow Cytometry*, Wiley-Liss, 2003.
2 C. Wyatt Shields Iv, C. D. Reyes and G. P. Lopez, *Lab Chip*, 2015, **15**, 1230–1249.
3 W. L. Ung, K. Mutafopulos, P. Spink, R. W. Rambach, T. Franke and D. A. Weitz, *Lab Chip*, 2017, **17**, 4059–4069.
4 T. Franke, S. Braunmuller, L. Schmid, A. Wixforth and D. A. Weitz, *Lab Chip*, 2010, **10**, 789–794.
5 T.-H. Wu, Y. Chen, S.-Y. Park, J. Hong, T. Teslaa, J. F. Zhong, D. Di Carlo, M. A. Teitell and P.-Y. Chiou, *Lab Chip*, 2012, **12**, 1378–1383.
6 M. M. Wang, E. Tu, D. E. Raymond, J. M. Yang, H. Zhang, N. Hagen, B. Dees, E. M. Mercer, A. H. Forster, I. Kariv, P. J. Marchand and W. F. Butler, *Nat. Biotechnol.*, 2004, **23**, 83.
7 L. Ren, S. Yang, P. Zhang, Z. Qu, Z. Mao, P.-H. Huang, Y. Chen, M. Wu, L. Wang, P. Li and T. J. Huang, *Small*, 2018, 1801996.
8 C. W. t. Shields, C. D. Reyes and G. P. Lopez, *Lab Chip*, 2015, **15**, 1230–1249.
9 M. Eisenstein, *Nature*, 2006, **441**, 1179–1185.
10 J. M. Martel and M. Toner, *Sci. Rep.*, 2013, **3**, 3340.
11 D. Di Carlo, *Lab Chip*, 2009, **9**, 3038–3046.
12 Y. Chen, T.-H. Wu, Y.-C. Kung, M. A. Teitell and P.-Y. Chiou, *Analyst*, 2013, **138**, 7308–7315.
13 Y. Chen, A. J. Chung, T. H. Wu, M. A. Teitell, D. Di Carlo and P. Y. Chiou, *Small*, 2014, **10**, 1746–1751.
14 D. J. Collins, A. Neild and Y. Ai, *Lab Chip*, 2016, **16**, 471–479.
15 Z. Ma, Y. Zhou, D. J. Collins and Y. Ai, *Lab Chip*, 2017, **17**, 3176–3185.
16 S. Sakuma, Y. Kasai, T. Hayakawa and F. Arai, *Lab Chip*, 2017, **17**, 2760–2767.
17 L. Schmid, D. A. Weitz and T. Franke, *Lab Chip*, 2014, **14**, 3710–3718.
18 A. A. S. Bhagat, S. S. Kuntaegowdanahalli and I. Papautsky, *Lab Chip*, 2008, **8**, 1906–1914.
19 S. S. Kuntaegowdanahalli, A. A. Bhagat, G. Kumar and I. Papautsky, *Lab Chip*, 2009, **9**, 2973–2980.
20 G. Guan, L. Wu, A. A. Bhagat, Z. Li, P. C. Y. Chen, S. Chao, C. J. Ong and J. Han, *Sci. Rep.*, 2013, **3**, 1475.
21 J. M. Martel and M. Toner, *Annu. Rev. Biomed. Eng.*, 2014, **16**, 371–396.
22 W. R. Dean, *The London, Edinburgh, and Dublin Philosophical Magazine and Journal of Science*, 1927, **4**(20), 208–223.
23 W. R. Dean, *The London, Edinburgh, and Dublin Philosophical Magazine and Journal of Science*, 1928, **5**(30), 673–695.
24 A. E. Hasni, K. Göbbels, A. L. Thiebes, P. Bräunig, W. Mokwa and U. Schnakenberg, *Procedia Eng.*, 2011, **25**, 1197–1200.
25 J. F. Edd, D. Di Carlo, K. J. Humphry, S. Köster, D. Irimia, D. A. Weitz and M. Toner, *Lab Chip*, 2008, **8**, 1262–1264.
26 S. Chung, S. J. Park, J. K. Kim, C. Chung, D. C. Han and J. K. Chang, *Microsyst. Technol.*, 2003, **9**, 525–533.
27 G. Destgeer, B. H. Ha, J. Park, J. H. Jung, A. Alazzam and H. J. Sung, *Phys. Procedia*, 2015, **70**, 34–37.
28 H. Yatsuda, Y. Takeuchi and S. Yoshikawa, *IEEE Int. Ultrason. Symp.*, 1990, **1**, 61–66.
29 L. Solie, *IEEE Int. Ultrason. Symp.*, 1998, **1**, 27–37.
30 H. Yatsuda, K. Noguchi and K. Yamanouchi, *Jpn. J. Appl. Phys.*, 2000, **39**, 3041–3044.
31 X. Ding, J. Shi, S. C. Lin, S. Yazdi, B. Kiraly and T. J. Huang, *Lab Chip*, 2012, **12**, 2491–2497.
32 X. Ding, P. Li, S.-C. S. Lin, Z. S. Stratton, N. Nama, F. Guo, D. Slotcavage, X. Mao, J. Shi, F. Costanzo and T. J. Huang, *Lab Chip*, 2013, **13**, 3626–3649.
33 T. Frommelt, D. Gogel, M. Kostur, P. Talkner, P. Hanggi and A. Wixforth, *IEEE Trans. Ultrason. Ferroelectr. Freq. Control*, 2008, **55**, 2298–2305.
34 L. Y. Yeo and J. R. Friend, *Biomicrofluidics*, 2009, **3**, 12002.
35 H. Bruus, *Lab Chip*, 2012, **12**, 1014–1021.
36 G. Wang, C. Turbyfield, K. Crawford, A. Alexeev and T. Sulchek, *Microfluid. Nanofluid.*, 2015, **19**, 987–993.
37 G. Destgeer, K. H. Lee, J. H. Jung, A. Alazzam and H. J. Sung, *Lab Chip*, 2013, **13**, 4210–4216.
38 V. Skowronek, R. W. Rambach, L. Schmid, K. Haase and T. Franke, *Anal. Chem.*, 2013, **85**, 9955–9959.
39 R. Shilton, M. K. Tan, L. Y. Yeo and J. R. Friend, *J. Appl. Phys.*, 2008, **104**, 014910.
40 W. Qi, C. Zhao, L. Zhao, N. Liu, X. Li, W. Yu and L. Wei, *Cancer Cell Int.*, 2014, **14**, 3.
41 D. L. Garner, K. M. Evans and G. E. Seidel, in *Spermatogenesis: Methods and Protocols*, ed. D. T. Carrell and K. I. Aston, Humana Press, Totowa, NJ, 2013, pp. 279–295, DOI: 10.1007/978-1-62703-038-0_26.
42 C. Alix-Panabières and K. Pantel, *Lab Chip*, 2014, **14**, 57–62.

43 *Designing your own device*, Stanford Microfluidics Foundry, Stanford, 2015.
44 L. Schmid and T. Franke, *Lab Chip*, 2013, **13**, 1691–1694.
45 D. P. a. E. G. S. P. Morgan, *Surface acoustic wave filters: with applications to electronic communications and signal processing*, Academic Press, Oxford, 2007, 2nd ed.
46 S. Jen and R. Bobkowski, *2000 Ieee Ultrasonics Symposium Proceedings, Vols 1 and 2*, 2000, vol. 1, pp. 269–273.
47 J. J. Agresti, E. Antipov, A. R. Abate, K. Ahn, A. C. Rowat, J.-C. Baret, M. Marquez, A. M. Klibanov, A. D. Griffiths and D. A. Weitz, *Proc. Natl. Acad. Sci. U. S. A.*, 2010, **107**, 4004.
48 L. Mazutis, J. Gilbert, W. L. Ung, D. A. Weitz, A. D. Griffiths and J. A. Heyman, *Nat. Protoc.*, 2013, **8**, 870–891.